CHEMPHYSCHEM

Role of Temperature in Controlling Performance of Photorefractive Organic Glasses

Oksana Ostroverkhova,*[a,c] Meng He,[b] Robert J. Twieg,[b] and W. E. Moerner*[a]

We present a detailed temperature-dependence study of dielectric, birefringent, conductive, and photorefractive (PR) properties of high-performance low-molecular weight organic glasses that contain 2-dicyanomethylene-3-cyano-2,5-dihydrofuran (DCDHF) derivatives. DCDHF organic glasses sensitized with C_{60} exhibit high two-beam coupling gain coefficients in the red-wavelength region. However, in the best performing DCDHF glasses at room temperature the PR dynamics are limited by slow molecular reorientation in the electric field. While orientational and, therefore, PR speed can be significantly improved by increasing the temperature above the glass-transition temperature of the material, the steady-state performance may worsen. Comprehensive study of the temperature dependence of various processes, which contribute to the PR effect in DCDHF glasses, clarifies the limiting factors and allows for optimization of the overall PR performance.

KEYWORDS:

dark current · holography · monolithic glasses · nonlinear optics · photoconducting materials · photorefractive organic materials

1. Introduction

The photorefractive (PR) effect refers to a refractive index change under nonuniform illumination via space–charge field formation and electro-optic nonlinearity.[1] PR materials have gained considerable interest due to their potential applications such as image processing, optical data storage, optical limiting, and many others.[2] Since the first observation of the PR effect in a $LiNbO_3$ inorganic crystal in 1967,[3] in 2-(cyclooctylamino)-5-nitropyridine (COANP) doped with 7,7,8,8-tetracyanoquinodimethane (TCNQ) organic crystal in 1990,[4] and in bisphenol A diglycidyl diether 4-nitro-1,2-phenylenediamine (bisA-NPDA) doped with (diethylamino)benzaldehyde diphenylhydrazone (DEH) polymer composite in 1991,[5] substantial fundamental and applied research has been directed toward understanding the mechanism of the PR effect in various materials and utilizing the PR properties of the materials in applications.[1, 6, 7] PR organic materials, particularly polymers and glasses, are of technological interest due to their low cost, easy processing and chemical tunability.[8]

The PR effect in organic materials is a complicated process, in which the space–charge field forms through charge photogeneration, carrier transport and trapping, followed by the refractive index change due to the electro-optic effect and chromophore reorientation in the space–charge field.[1] Therefore, the PR material should possess both photoconductive and nonlinear optical (NLO) properties. There are several classes of organic materials utilized in PR studies.[6, 8, 9] The most well studied class is PR polymer composites, in which the polymer functions as a charge-transporting network, a NLO chromophore provides electro-optic nonlinearity, a sensitizer assists in charge generation, and in most cases a plasticizer is used to lower the glass-transition temperature (T_g) of the composite to facilitate chromophore reorientation and to take advantage of the orientational enhancement effect.[10] Numerous studies have been conducted to clarify the role of each constituent in various mechanisms, which contribute to the overall PR performance.[11–19] The best PR polymer composites are characterized by millisecond-response times,[20] two-beam coupling gain coefficients of $\approx 400\,cm^{-1}$,[21] and diffraction efficiencies of $\approx 100\,\%$[22] at applied electric fields of $\approx 100\,V\,\mu m^{-1}$.

Less explored PR organic materials include bifunctional systems, in which the NLO moieties are attached as side groups to the polymer backbone[23, 24] or to an amorphous, hole-transporting molecule,[25] fully functionalized systems,[26, 27] and monolithic organic glasses.[28–31] The advantages of such systems in comparison with polymer composites are high concentrations of NLO moieties that create large nonlinearity without phase separation, high concentration of charge transport sites, and no inert volume, which in most polymer composites is introduced by a plasticizer. The best performing multifunctional systems exhibit net gain coefficients of $\approx 200\,cm^{-1}$ at $30\,V\,\mu m^{-1}$,[31] $\approx 100\,\%$ diffraction efficiencies,[24] and have millisecond-response times.[30]

[a] *Prof. W. E. Moerner, Dr. O. Ostroverkhova*
Department of Chemistry, Stanford University
Stanford, CA 94305-5080 (USA)
Fax: (+1) 650-725-0259
E-mail: wmoerner@stanford.edu
E-mail: oksanao@stanford.edu

[b] *Dr. M. He, Prof. R. J. Twieg*
Department of Chemistry, Kent State University
Kent, OH 44242 (USA)

[c] *Current address:*
Department of Physics
University of Alberta (Canada)

  DOI: 10.1002/cphc.200200633

We have previously reported improved PR properties that can be achieved in monolithic glasses,[31, 32] which contain 2-dicyanomethylene-3-cyano-2,5-dihydrofuran (abbreviated as DCDHF) derivatives. High net gain coefficients ($\approx 310\ cm^{-1}$ at an electric field of $40\ V\,\mu m^{-1}$ and a wavelength of 676 nm[31] and $\approx 370\ cm^{-1}$ at $45\ V\,\mu m^{-1}$ at 830 nm[33] in the best performing DCDHF glasses) were observed. However, the PR dynamics are slow, ranging between 0.02 s^{-1} and 2 s^{-1} at 676 nm and between 0.005 s^{-1} and 0.2 s^{-1} at 830 nm, depending on material. While low PR speed at 830 nm in most of these glasses was attributed to low charge photogeneration efficiency, the low PR speed at 676 nm in most cases was shown to be orientationally limited.[31] It is well-known that chromophore reorientational dynamics are highly dependent on the T_g of the material.[34–37] Thus, by adjusting the T_g or the temperature of the measurement (T) it should be possible to achieve better orientational, and therefore, PR response times.

In this article, we present a comprehensive study of the temperature dependence of orientational as well as dielectric, photoconductive, and PR properties of several DCDHF-containing monolithic glasses. By means of temperature-dependence studies, we seek: (1) clarification of the nature of various processes such as orientational dynamics, conductivity, and trapping in our glasses; (2) comparison of various mechanisms leading to the PR effect in monolithic glasses with similar mechanisms in polymer composites; (3) understanding of the factors that limit steady-state and dynamic performance of our materials; (4) the ability to fine-tune the PR properties by adjusting the temperature in the region around T_g ($0.98T_g < T < 1.1T_g$).

2. Results and Discussion

2.1. Materials

For our temperature-dependence studies we chose three DCDHF-containing glasses: DCDHF-6-CF3 (**1**), DCDHF-8/DCDHF-6-C7M (1:1 wt mixture) (**2**) and DCDHF-6/DCDHF-6-C7M (1:1 wt mixture) (**3**), all sensitized with 0.5 wt% C_{60} (Figure 1). Further experimental details are presented in the Experimental Section. These glasses exhibited good thermal stability and did not recrystallize upon heating, in contrast with many other DCDHF glass-forming derivatives, including neat DCDHF-6, DCDHF-8, and DCDHF-6-C7M, which are thermally unstable.[31, 32]

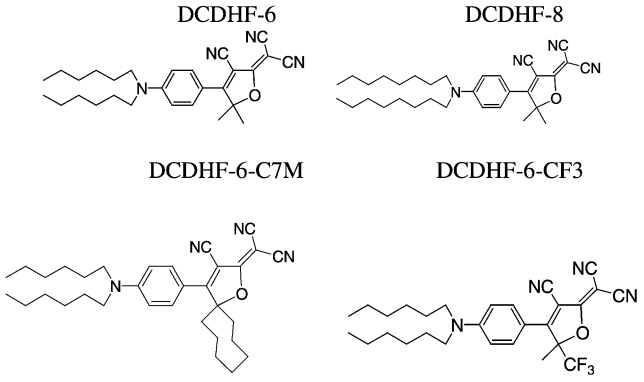

Figure 1. *Molecular structures of DCDHF-based chromophores used in photorefractive studies of temperature dependence.*

The composites **1** – **3** possessed slightly different glass transition temperatures of 17 °C (compound **1**), 20 °C (composite **2**) and 23 °C (composite **3**),[31] which allowed us to compare various parameters obtained in composites **1** – **3** at the same relative to T_g temperatures and to generalize the observed behavior to several DCDHF glasses as opposed to one particular composition.

2.2. Dielectric Properties

To investigate dielectric properties of our materials, we performed dielectric relaxation spectroscopy experiments.[38] Real and imaginary parts of the dielectric permittivity (ε' and ε'', respectively) were determined as functions of frequency of the ac (alternating current) electric field applied across the sample. Figure 2 shows the frequency dependence of ε' and ε'' obtained in the composite **3**/C_{60} in the frequency range of 10 mHz – 1 MHz at various temperatures.

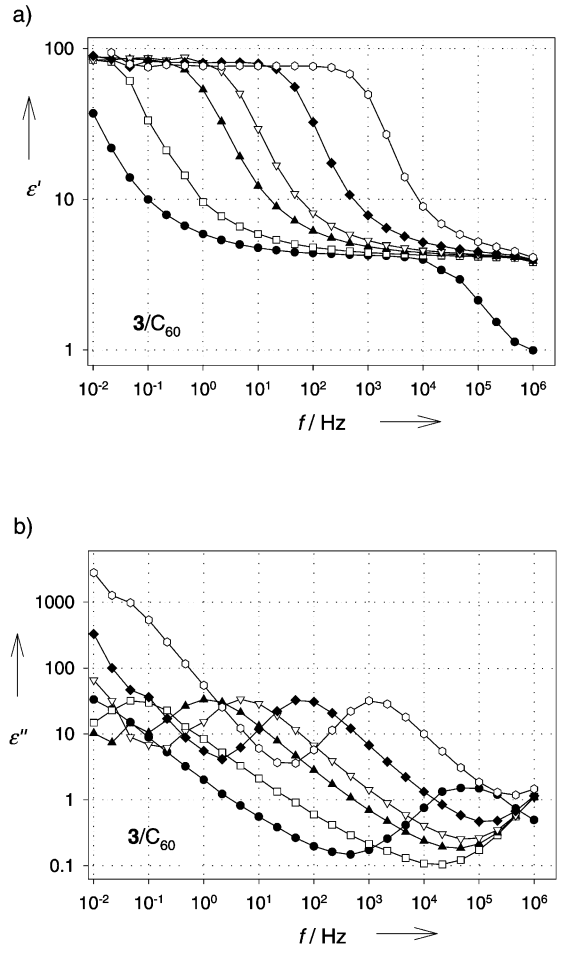

Figure 2. *Frequency dependence of dielectric permittivity at various temperatures: a) real part (dielectric constant); b) imaginary part (dielectric loss); ● 20 °C, □ 24 °C, ▲ 28 °C, ▽ 33 °C, ◆ 39 °C, ○ 49 °C.*

The angular frequency dependence of dielectric permittivity can be represented as follows [Equation (1)]:

$$\varepsilon(\omega) = \varepsilon'(\omega) - i\varepsilon''(\omega) = \sum_k \Delta\varepsilon_k(\omega) + \varepsilon_\infty - i\sigma_{dc}/\omega\varepsilon_0 \quad (1)$$

where σ_{dc} is the dc (direct current) conductivity, ε_0 is the permittivity of vacuum, and ε_∞ is the high-frequency permittivity. Each dielectric mode $\Delta\varepsilon_k(\omega)$ can be described by semi-empirical Havriliak – Negami (H-N) function [Equation (2)]:[39]

$$\Delta\varepsilon_k(\omega) = \frac{\Delta\varepsilon_k}{[1 + (i\omega\tau_{0k})^{1-\alpha_k}]^{\beta_k}} \quad (2)$$

where $\Delta\varepsilon_k$ is the dielectric strength of each mode, τ_{0k} is a relaxation time, α_k is a parameter that describes symmetric broadening of the relaxation peak ($0 < \alpha_k \leq 1$) and β_k is a parameter related to asymmetric broadening at higher frequencies ($0 < \beta_k \leq 1/\alpha_k$). The case of $\alpha = 0$, $\beta = 1$ corresponds to a simple Debye-type relaxation.[38]

In the studied frequency range, the dielectric permittivity of the composite **3**/C_{60} exhibited several features. At temperatures several degrees below T_g a higher frequency peak (with a maximum at a frequency of $\approx$70 kHz at 20 °C, as seen in Figure 2b) is observed in the dielectric loss factor (ε''). Also, an increase in ε'' is observed at lower frequencies (below $\approx$100 Hz), which reflects the onset of large-scale motion at temperatures close to T_g. At temperatures above T_g, the lower frequency (primary relaxation) peak in the dielectric absorption spectrum is clearly observed (Figure 2b). The primary relaxation occurs faster at elevated temperatures, so that the frequency of the loss maximum changes from $\approx$80 mHz at 24 °C to $\approx$1 kHz at 49 °C. Similarly, the dielectric loss observed at sub-T_g temperatures at frequencies $\approx$10 – 100 kHz (secondary relaxation) occurs at higher frequencies as the temperature increases and, already at T_g, the frequency at the peak maximum is beyond the upper limit of our experimental scale (1 MHz). The dielectric loss due to secondary relaxation is characterized with a lower dielectric strength ($\Delta\varepsilon$) and broader distribution of relaxation times in comparison with the one due to primary relaxation. Qualitatively, the temperature and frequency dependencies of the primary and secondary relaxations in the compound **3**/C_{60} are similar to those of α and β relaxations, respectively, observed in polymers.[38, 40] In DCDHF glasses we associate the primary relaxation with reorientation of DCDHF chromophores in the ac field. The secondary relaxation could reflect a local motion of side groups. However, it could also be due to molecular interactions, intrinsic for the DCDHF glass. In order to understand the nature of secondary relaxation in the DCDHF glasses, more studies are required.[41]

At higher temperatures (above 33 °C in Figure 2b), a significant increase in dielectric loss factor ε'' is observed at low frequencies. We attribute this to ionic conductivity (σ_{dc}), which drastically increases as a function of temperature as confirmed by our independent measurements of the dc current (see Section 2.4.1.) and contributes to a complex dielectric permittivity, namely, dielectric loss ε'', in accordance with Equation (1).

To analyze the dielectric relaxation spectra, it is conventional to use complex-plane plots of the dielectric constant parametric in radian frequency.[42] In the Debye single-time relaxation model,[38] such plots yield a semi-circle. Dispersion curves of most polymers depart from a semi-circle and are better characterized with the H-N equation [Equation (2)]. In our further analysis, we concentrate on the lower frequency dielectric mode (primary relaxation), which was attributed to the DCDHF chromophore reorientation in the ac electric field. By fitting our data with the H-N equation, we determined the dielectric strength $\Delta\varepsilon$, relaxation time τ_0, and parameters α and β of Equation (2) at various temperatures. Figure 3a shows a

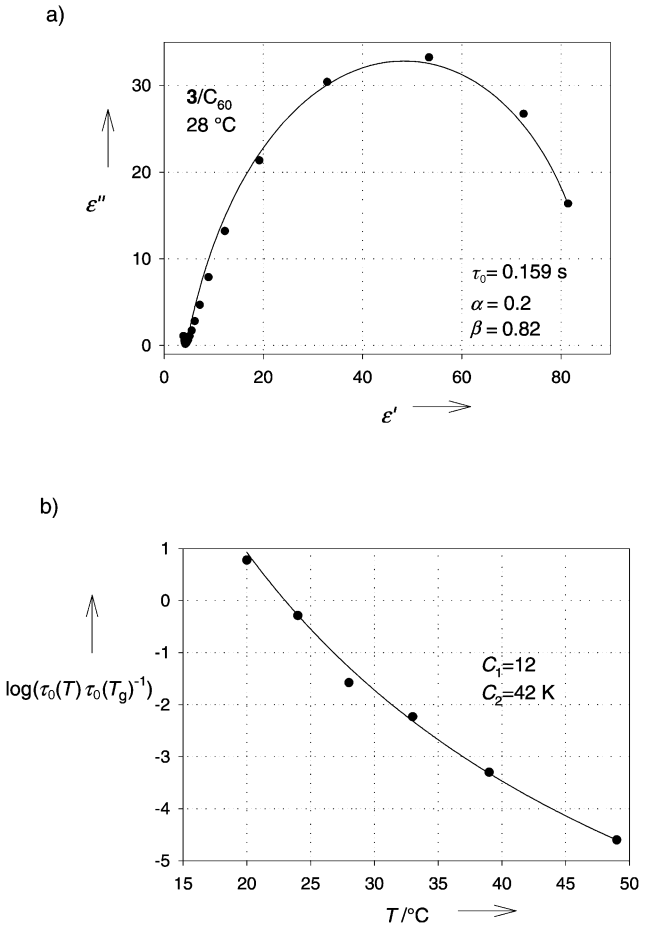

Figure 3. *a) Complex plane plot of the dielectric constant obtained in composite* ***3****/C_{60} at 28 °C (● experimental data). Solid line (——) represents the fit to the Havriliak – Negami equation. b) Dielectric relaxation time normalized to the value at T = T_g as a function of temperature (● experimental data). Solid line (——) represents the fit to the WLF equation.*

complex-plane plot of the dielectric constant obtained in the composite **3**/C_{60} at a temperature of 28 °C, fitted with the H-N equation. At this temperature, the fit yielded a dielectric strength $\Delta\varepsilon = 82$, a relaxation time $\tau_0 = 0.159$ s, and parameters $\alpha = 0.2$ and $\beta = 0.82$. The high value of dielectric strength reflects the highly polar environment, as expected in the composite **3**/C_{60}, 99.5 % of which is a mixture of DCDHF-6 and DCDHF-6-C7M chromophores (dipole moments $\mu = 38 \times 10^{-30}$ C m and

36×10^{-30} C m, respectively[43]). The parameter $\alpha = 0.2$ is in the range of those typically observed in polymers under similar conditions (for example $\alpha = 0.205$ in polycarbonate (PC) at a temperature of 164 °C[42]). The parameter $\beta = 0.82$ is higher than typical values of 0.2 – 0.6 obtained in polymers at and above T_g (for example $\beta = 0.285$ in PC at a temperature of 164 °C[42]). Since the parameters $\alpha \neq 0$ and $\beta \neq 1$, our system cannot be described by the simple Debye model of independently rotating dipoles, and thus, some cooperativity in dipole orientation is involved. At all studied temperatures above T_g, the parameters α and β remained the same within ≈5%, which suggests temperature-independent cooperativity between individual dipoles.

In polymers and glasses at temperatures above T_g, the temperature dependence of various parameters such as viscosity, elasticity, and characteristic relaxation times is described well by the Williams – Landel – Ferry (WLF) model.[44] In the WLF model, the relaxation times at T_g and $T > T_g$ are related by the following expression [Equation (3)]:

$$\log\frac{\tau_0(T)}{\tau_0(T_g)} = -\frac{C_1(T - T_g)}{C_2 + T - T_g} \quad (3)$$

where C_1, C_2 are constants that depend on the free volume at T_g, the difference of the thermal expansion coefficients above and below T_g, and molecular size.[40] Figure 3b shows a fit of the WLF function [Equation (3)] to the temperature dependence of relaxation times obtained from H-N fits in the composite **3**/C_{60}; the fit is quite satisfactory. The WLF fit yielded values of $C_1 = 12$ and $C_2 = 42$ K, which are in the range of values typical for polymers and other glasses.[37]

2.3. Birefringent Properties

2.3.1. Steady-State Birefringence

We have previously reported high birefringence values due to chromophore orientation in the electric field that are obtained in transmission ellipsometry experiments in DCDHF-containing glasses.[31] In particular, at a temperature of ≈21 °C composites **1** – **3** exhibited close to quadratic electric field dependence of the index change and yielded birefringence values Δn_{BR} (100 s) of ≈0.001 – 0.006 at time $t = 100$ s after the step-function electric field of 25 V μm^{-1} was applied.[31] Here, we investigate how the steady-state birefringence values change with temperature ranging from 19 °C (within 4 °C around T_g for all the compounds) to 55 °C (≈35 °C above T_g).

In polar, organic materials, the electric field-induced birefringence (Δn_{BR}) can be viewed as a change in the anisotropy of the first- and second-order susceptibilities due to the chromophore alignment in the electric field.[10]When describing chromophore alignment in the electric field at temperatures above T_g, it is conventional to apply the oriented gas model,[45] which assumes freely rotating, noninteracting molecules. Then, in the case of an azimuthally symmetric system, the electric field poling process is described by the Debye rotational diffusion equation for an angular molecular distribution function f [Equation (4)]:[46]

$$\frac{1}{D}\frac{\partial f(\theta,t)}{\partial t} = \frac{1}{\sin\theta}\frac{\partial}{\partial\theta}\left\{\sin\theta\left[\frac{\partial}{\partial\theta}f(\theta,t) + \frac{1}{kT}\frac{\partial U}{\partial\theta}f(\theta,t)\right]\right\} \quad (4)$$

where the energy U is given as $U = -\mathbf{m}^*\mathbf{E}_0 = -m^*E_0\cos\theta$, where m^* is a dressed dipole moment, E_0 is the electric field, and θ the angle between the electric field and the dipole moment. In the general case, the solution of Equation (4) can be presented in terms of spherical modified Bessel functions.[47] However, in the low-field limit, a simplified form of the solution can be assumed,[45] and the electric field-induced change in birefringence can be written as follows [Equation (5)]:[1, 10, 48]

$$\Delta n_{BR}(T) = \frac{1}{2\varepsilon_0 n}\left(\frac{3}{2}C_{BR}(T) + \frac{2}{3}C_{EO}(T)\right)E_0^2$$
$$C_{BR} = \frac{2}{45}Nf_\infty\delta\alpha\left(\frac{\mu}{kT}\right)^2 \quad (5)$$
$$C_{EO} = Nf_0f_\infty^2\frac{\beta\mu}{5kT}$$

where N is the chromophore concentration, f_0, f_∞ are local field factors, $\delta\alpha$ is the polarizability anisotropy, β is the molecular first hyperpolarizability, and μ is the dipole moment.

According to Equations (5), the steady-state electric field-induced birefringence (Δn_{BR}) is expected to behave as a second-order polynomial of (1/T), that is, a decrease as the temperature increases due to thermal disruption of the chromophore alignment. Figure 4 shows the temperature dependence of birefringence (Δn_{BR}) obtained in composites **1** – **3**/C_{60} at an electric field

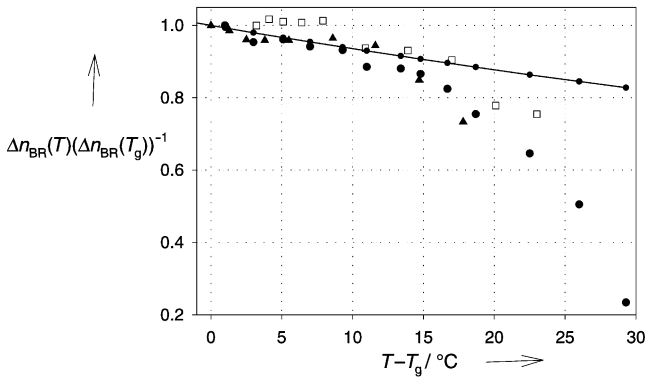

Figure 4. *Birefringence of the composites* ***1*** *–* ***3****/C_{60} normalized at its value at* $T = T_g$ *as a function of temperature [□* ***1****/C_{60}, ▲* ***2****/C_{60}, ●* ***3****/C_{60}]. Line with symbols shows the temperature dependence of the birefringence calculated from oriented gas model for the composite* ***3****/C_{60}.*

of 25 V μm^{-1}, normalized at the value at $T = T_g$. Indeed, in all three composites, the birefringence decreased as the temperature increased. In the range of temperatures $T_g < T < T_g + 10$ °C, the experimentally measured temperature dependence approximately follows the one calculated from Equations (5), using the polarizability $\delta\alpha$, the hyperpolarizability β, and the dipole moment μ, which is determined from electroabsorption measurements of the DCDHF glasses[43] (line with symbols in Figure 4 for the composite **3**/C_{60}). For other DCDHF-containing composites similar dependencies are predicted (not shown), since they possess similar molecular constants $\delta\alpha$, β, and μ.[43] Therefore, the strong decline in birefringence, which is observed in all

composites starting at temperatures $\approx 15\,^{\circ}C$ above T_g, cannot be described in the framework of the oriented gas model.

Since DCDHF glasses consist of densely packed, dipolar molecules and thus represent a highly interacting system, additional temperature-dependent effects due to dipole – dipole interactions may appear. It has been shown that dipole – dipole interactions change the order parameters $\langle \cos^n\theta \rangle$ and relaxation times.[45, 49, 50] In particular, in the weak electric field limit second-order nonlinear susceptibilities $\chi^{(2)}_{zzz} \sim \langle \cos^3\theta \rangle$, $\chi^{(2)}_{zxx} \sim \langle \cos\theta \rangle - \langle \cos^3\theta \rangle$ are enhanced due to dipole – dipole interactions by the Kirkwood factor $g_K = \langle M^2 \rangle / N_0 \mu^2$, where M is a total dipole moment of the sample, N_0 is a number of molecules, and μ is a dipole moment of the molecule [Equation (6)]:

$$\chi^{(2)}_{d\text{-}d} = g_K \chi^{(2)}_0 \tag{6}$$

where $\chi^{(2)}_{d\text{-}d}$ is the susceptibility in the system of interacting dipoles and $\chi^{(2)}_0$ is the susceptibility of oriented gas. The Kirkwood factor g_K is larger than unity and depends on molecular arrangement in the bulk.[50] The electric field-induced birefringence (Δn_{BR}) is a combination of $\langle \cos\theta \rangle$, $\langle \cos^2\theta \rangle$, and $\langle \cos^3\theta \rangle$ and therefore, is similarly affected by dipole – dipole interactions. In polymers and glasses above T_g, translational and rotational diffusion processes, which change molecular arrangement and therefore, intermolecular interaction potential, are strongly temperature dependent. Thus, the Kirkwood factor in Equation (6) may depend on temperature. According to Kirkwood's theory, the macroscopic dielectric constant is related to the molecular dipole moment as follows Equation (7):[38]

$$\frac{(\varepsilon(0) - \varepsilon_\infty)(2\varepsilon(0) + \varepsilon_\infty)}{\varepsilon(0)(\varepsilon_\infty + 2)^2} = g_K \frac{\mu^2 N}{9\varepsilon_0 k_B T} \tag{7}$$

where ε_∞, $\varepsilon(0)$, and ε_0 are the high-frequency, static and vacuum-dielectric permittivities, respectively, N is the chromophore concentration, and μ is the molecular dipole moment. Our dielectric measurements (Section 2.2.) showed that in DCDHF glasses the static dielectric constant $\varepsilon(0)$ does not appreciably change with temperature (ε' at low frequencies in Figure 2a). Thus, as the left-hand side of Equation (7) is independent of temperature, the Kirkwood factor g_K would exhibit a $\approx 12\%$ *increase* as the temperature increases from 19 °C (292 K) to 55 °C (328 K). Therefore, strong dipole – dipole interactions would not account for the observed strong decrease of birefringence at higher temperatures (Figure 4).

Firestone et al.[51] observed a similarly strong decrease in the second-order susceptibility ($\chi^{(2)}$) at temperatures above T_g in a poled chromophore-functionalized polymer. The stronger than predicted by the oriented gas model temperature dependence at these temperatures was attributed to conductivity and space – charge field effects that significantly increased above T_g, reducing the effective electric field.[51, 52] This could be the explanation for the observed birefringence decrease at temperatures above T_g in DCDHF glasses, as a strong increase of dark conductivity in this temperature region was confirmed by our dc conductivity measurements (Section 2.4.1.).

Finally, we note that there is spectroscopic evidence of dimer formation in DCDHF glasses.[53] Dimers can serve as deep traps for the charge[54] and when charged, exhibit such properties as the appearance of a dipole moment perpendicular to the monomer axis,[55] which leads to additional interactions among charged dimers, monomers, and electric field. These interactions could be also temperature dependent, which would further complicate the physical picture.

2.3.2. Orientational Dynamics

The orientational speed k_{BR} was determined by either single-exponential ($\Delta n_{BR} \sim 1 - \exp[-k_{BR}t]$) or stretched Kohlrausch – Williams – Watts (KWW) exponential ($\Delta n_{BR} \sim 1 - \exp[-(k_{BR}t)^{\beta_s}]$) fits to the birefringence rise due to chromophore alignment in response to a step-function electric field. Figure 5a shows the birefringence rise transients (symbols) obtained in composite **3**/C_{60} at an electric field of 25 V μm^{-1} at various temperatures, normalized to the steady-state value (100 s). As the temperature increases, the orientational speed (k_{BR}) increases dramatically with a maximal increase of more than an order of magnitude over the temperature range of only $\approx 4\,^{\circ}C$ at around T_g. Figure 5b shows the dependence of k_{BR} on the temperature

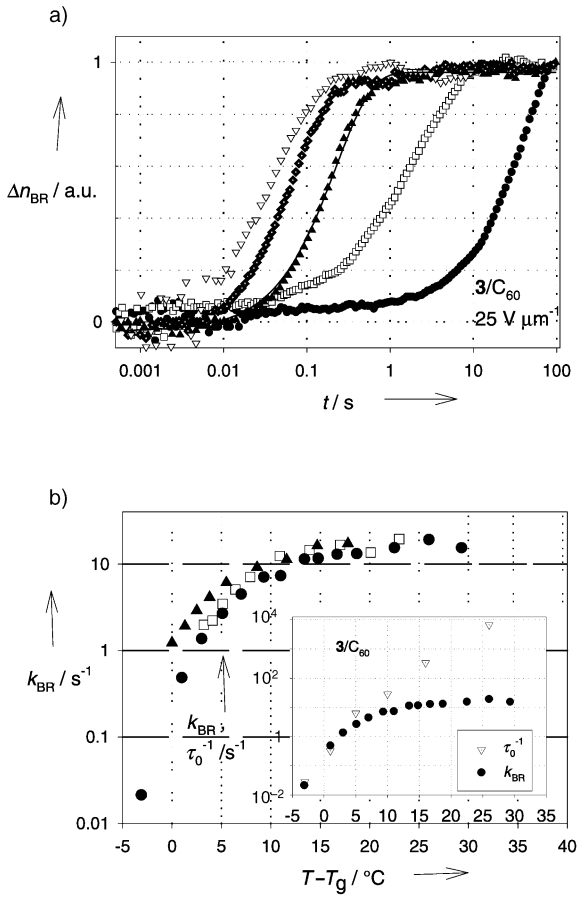

Figure 5. *a) Birefringence rise at various temperatures in* **3**/C_{60} (● *20.3 °C,* □ *24 °C,* ▲ *30 °C,* ◆ *39.7 °C,* ▽ *49 °C). Single-exponential fit to the transient obtained at 30 °C is also shown (——); b) Orientational speed (k_{BR}) obtained in several DCDHF composite (□* **1**/C_{60}, ▲ **2**/C_{60}, ● **3**/C_{60}*) as a function of relative to T_g temperature. Inset shows k_{BR} and inverse dielectric relaxation time τ_0^{-1} as functions of $T - T_g$ in* **3**/C_{60}.

relative to T_g, obtained in the composites **1** – **3**/C_{60}. The temperature dependence of the orientational dynamics in all composites is strong with at least one order of magnitude increase in k_{BR} at temperatures $\approx 10\,^{\circ}C$ above T_g in comparison with the values of k_{BR} obtained at T_g. All three composites exhibited universal behavior of orientational speed, which indicates that the chromophore reorientational dynamics in DCDHF glasses are determined by their thermodynamic state, namely, the temperature relative to T_g, or $T - T_g$, rather than by the chemical nature of the chromophores. This behavior is similar to that observed in polymer guest – host systems.[34, 56] However, in contrast with polymer composites, in which the orientational processes are dispersive with weakly temperature-dependent KWW parameters,[44, 57] DCDHF glasses show dispersivity at temperatures below T_g ($\beta_s \approx 0.6$ at a temperature of $\approx 19\,^{\circ}C$ for the composite **3**/C_{60}), but exhibit single-exponential behavior at temperatures above T_g. The single-exponential fit of the birefringence rise obtained in the composite **3**/C_{60} at a temperature of $30\,^{\circ}C$ is illustrated in Figure 5a (solid line).

To better understand the temperature dependence of birefringence rise times, we compare them with the dielectric relaxation times (Section 2.2.). Over the years, in studies of relaxation processes in polymer and simple organic liquids, considerable attention was devoted to identifying the factors that influence the relaxation dynamics[51, 52] and investigating relationships between relaxation times obtained with various techniques such as dielectric relaxation spectroscopy, NMR spectroscopy, photon correlation spectroscopy, light scattering, second harmonic generation (SHG), etc.[34, 35, 40, 44] Factors that affect the relaxation dynamics include physical aging of the material, poling time, electric field strength, dipole – dipole interactions, and others.[49, 51, 52] Combinations of several factors complicate the data tractability. For example, in poled polymers, relaxation times obtained in SHG experiments were reported as both increasing[58] and decreasing[51, 59] functions of the poling field strength. Therefore, it is important to take into account experimental conditions when comparing the data obtained by different techniques.

The inset of Figure 5b shows orientational speed k_{BR} that is measured in the transient ellipsometry experiment and inverse dielectric relaxation time τ_0^{-1} obtained from dielectric loss measurements (Section 2.2.) in the composite **3**/C_{60} as a function of $T - T_g$. Since different order parameters are measured in these two experiments ($\langle \cos^2\theta \rangle$ dominates in birefringence transients and $\langle \cos\theta \rangle$ in dielectric spectroscopy), one expects that the time constants obtained from these measurements may differ up to a factor of three.[47] However, a much greater deviation of k_{BR} from τ_0^{-1} is observed at temperatures above $\approx T_g + 10\,^{\circ}C$.

In guest – host polymers, Schussler et al.[60] observed much longer relaxation times obtained from SHG experiments compared with the dielectric relaxation times at all temperatures. Such a deviation of the chromophore reorientational dynamics measured by SHG from the polymer α-relaxation measured by dielectric spectroscopy was attributed to a difference in the magnitude of electric fields applied to a sample in these experiments (strong dc field in the case of SHG versus weak ac in the case of dielectric spectroscopy), which causes a different response of the material.[61] This is most likely not the case in DCDHF glasses, since such a discrepancy in time constants would be observed at all temperatures, while our time constants measured in ellipsometry and dielectric spectroscopy at temperatures around T_g are similar. Also, it has been previously reported that in organic glasses the time constants derived from SHG and dielectric relaxation experiments were consistent with each other.[62]

As discussed in Section 2.2., in the dielectric relaxation measured in DCDHF glasses at temperatures well above T_g two mechanisms that contribute to dielectric loss can be distinguished: higher frequency loss due to chromophore reorientation and lower frequency loss due to conductivity. In the transient ellipsometry experiments, which are carried out in the time domain, the observed reorientational dynamics could be affected by noninstantaneous space – charge field formation that is caused by the pronounced increase in dark conductivity at temperatures above $\approx T_g + 10\,^{\circ}C$ (Section 2.4.1.). This would confound true reorientational dynamics probed by dielectric spectroscopy and result in the difference in time constants measured by ellipsometry and dielectric relaxation techniques (inset of Figure 5b).

2.4. Conductivity

2.4.1. Dark Conductivity

Analysis of the origins of dark conductivity can be reduced to two main alternatives—whether the charge is generated in the bulk material or injected from the electrodes. Each case can be further split in two: (1) in the case of bulk generation, whether the transport is ionic or electronic and (2) in the case of charge injection, whether the transport is emission-limited or space – charge field-limited.[54] In amorphous, organic materials clarifying the mechanism of dark conductivity is not an easy task, since the conductivity is a complicated function of many parameters due to energetic and positional disorder[64] and the presence of impurities and various kinds of traps.[54] In order to assign the observed behavior of dark conductivity to a certain process, it is necessary to investigate the dependence of dark current on temperature, electric field, work function of the electrodes, etc.[54] Still, it could be hard to make unambiguous conclusions,[18] since several processes assume similar electric field and temperature dependencies.[65] In particular, several theoretical models for charge transport such as the disorder formalism, Poole – Frenkel effect, dipole trap model, and others[64] lead to the same type of electric field (E) dependence of dark current density (j) as in the case of charge injection due to Schottky emission:[65] $\ln j \sim \beta E^{1/2}$. Similarly, both electronic conduction, which is described by the polaron model, and ionic transport yield the same electric field dependence of the current density[65, 66] $j \sim \sinh(aE)$. Temperature dependencies can be obscured due to relatively narrow experimentally accessible temperature ranges[64] and electrode-work-function dependencies involve issues of sample preparation, purity, and other properties, which are not directly related to a material under study.

To probe the mechanisms of dark conductivity in DCDHF glasses, we measured the electric field and temperature dependence of the dark current. Dark conductivity (σ_d) of the composites **1** – **3**/C_{60} obtained at an electric field of 20 V μm^{-1} as a function of $T-T_g$ is shown in Figure 6. At temperatures

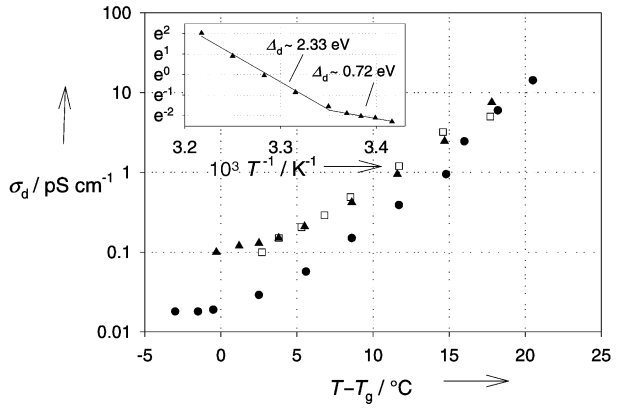

Figure 6. *Temperature dependence of dark conductivity obtained at an electric field of 20 V μm^{-1} in the compsites* ***1*** *–* ***3****/C_{60} (□* ***1****/C_{60}, ▲* ***2****/C_{60}, ●* ***3****/C_{60}). Inset shows Arrhenius fit to data for the compsite* ***2****/C_{60}.*

around T_g the dark conductivity $\sigma_d \leq 0.1$ pS cm^{-1}. Heating the composites to 15 – 20 °C above their T_g's leads to several orders of magnitude increase in dark conductivity. Two distinct regions with weaker and stronger temperature dependencies are observed at temperatures around T_g and above T_g, respectively (Figure 6, composites **2**/C_{60} and **3**/C_{60}). When plotted as a function of absolute temperature T and fitted with an Arrhenius-type function [Equation (8)]:

$$\sigma \sim \exp(-\Delta_d/kT) \quad (8)$$

the dark conductivity exhibits two activation energies (Δ_d) that correspond to these two temperature regions. The inset of Figure 6 shows the Arrhenius fit [Equation (8)] obtained for the composite **2**/C_{60}. In this material the fit yielded activation energies of $\Delta_d \approx 0.72$ eV at temperatures around T_g and $\Delta_d \approx$ 2.33 eV at higher temperatures.

One explanation for the observed behavior could be that at temperatures around T_g a change in the conductivity mechanism occurs. In polymers it has been shown that depending on the temperature and electric field, different processes would contribute to the dark current in the same material.[65, 67] However, a change in activation energy at temperatures around T_g is still a matter of controversy in the literature. For example, such a change was not observed in PVK-based composites;[18] however, a variety of polymers exhibited similar temperature dependence of dark conductivity[68–70] as we measured (Figure 6) and attributed the change in Δ_d to effects of electronic origin dominating below T_g and ionic hopping prevailing above T_g. Dark conductivity with activation energies ≈0.7 eV obtained in DCDHF glasses at temperatures around T_g could be explained by several electronic mechanisms such as Schottky emission (work function of ITO ≈4.6 – 4.9 eV and the ionization potentials of DCDHF compounds ≈5.54 – 5.61 eV) or trap activated transport.[64] At temperatures above T_g the conductivity with high activation energies (> 2 eV) could be attributed to transport of residual impurity ions, which might exist in DCDHF glasses as a result of the synthetic method used.[53]

The alternative interpretation of the temperature dependence of dark conductivity in DCDHF glasses (Figure 6) is that ionic transport dominates over other possible mechanisms at all temperatures.[66] In ref. [66] the conductivity of several polymers was studied as a function of temperature. Similar to DCDHF glasses a large change in activation energy (Δ_d) at temperatures around T_g was observed and explained by a change in the temperature dependence of the free volume at $T=T_g$: taking into account the change of the free volume at T_g removed the cusp in the log(σ_d) versus (1/T) plots.[66] The electric field dependence of ionic dark conductivity was described as [Equation (9)][66]

$$\sigma_d \sim \sinh(aE)/E \quad (9)$$

and the conductivity values ranged from 10^{-7} to 10^{-1} pS cm^{-1}, depending on the temperature.[66] The activation energies (Δ_d) of DCDHF glasses in both temperature regions (around and above T_g) are similar to those obtained in polymers.[66] Also, the electric field dependence of dark conductivity in DCDHF glasses could be reasonably fitted with Equation (9) at various temperatures relative to T_g (data not shown). Therefore, it is possible that ionic conduction is the origin of the dark current in DCDHF glasses in the studied temperature range. We note that at similar temperatures relative to T_g, the dark conductivity observed in DCDHF glasses is at least three orders of magnitude higher than that of polymers described in ref. [66] However, this could be due to a difference in ion concentration, mass, and other parameters that would affect the magnitude of conductivity.

2.4.2. Photoconductivity

The photoconductivity (σ_{ph}) is a function of photogenerated carrier density (ρ) and charge – carrier drift mobility (μ): $\sigma_{ph} = e\rho_i\mu$, where e is the charge of an electron. While the optical intensity dependence of σ_{ph} is associated only with the carrier density ρ the temperature dependence is contained in both the charge density and the mobility. In the charge density, temperature dependencies of photogeneration efficiency, trapping rate, recombination rate, and trap density are combined.[71] Temperature dependencies of charge density and mobility yield a complicated function for photoconductivity, which does not have features strong enough to allow determination of the origin of the observed dependence. To fully study the contribution of various processes to the overall photoconductivity temperature dependence, experiments should measure separately drift mobility, photogeneration efficiency, and other parameters,[18, 19, 64] measurements which are beyond the scope of this article.

The photoconductivity (σ_{ph}) of the compounds **1** – **3**/C_{60} was measured at a wavelength of 676 nm at an electric field of 20 V μm^{-1} as a function of light intensity and temperature. At

20 mW cm^{-2} the photoconductivity exhibited rather high values for low-molecular weight glasses of 0.4 – 2 pS cm^{-1}, depending on the material.[31] At all temperatures the photoconductivity was close to a linear function of light intensity in the range of intensities studied.[31] The temperature dependence of the photoconductivity at a light intensity of 20 mW cm^{-2} is shown in Figure 7. Although we could not reconstruct the contribution

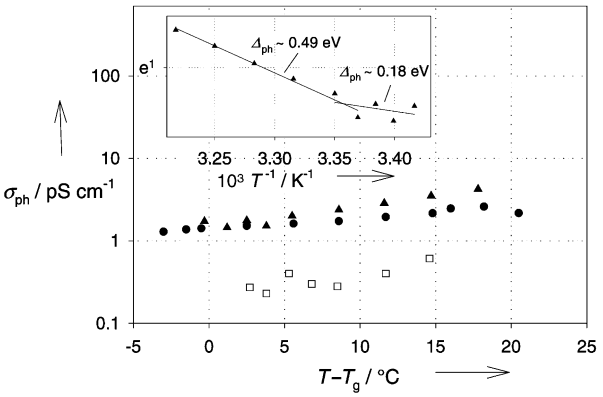

Figure 7. *Temperature dependence of photoconductivity obtained at an electric field of 20 V μm^{-1} and light intensity of 20 mW cm^{-2} in the composites **1** – **3**/C_{60} (□ **1**/C_{60}, ▲ **2**/C_{60}, ● **3**/C_{60}). Inset shows Arrhenius fit to data for the composite **2**/C_{60}.*

of each constituent of the photoconductivity to the dependence shown in Figure 7, we still performed the Arrhenius fit [$\sigma_{ph} \sim \exp(-\Delta_{ph}/kT)$] for easier comparison between dark and photoconductivity temperature dependencies. Similar to dark conductivity the temperature dependence of the photoconductivity is stronger at temperatures above T_g than around T_g, which is reflected in differences in activation energies in these temperature regions. Qualitatively, the observed temperature dependence of photocurrent in DCDHF glasses is similar to that of PVK-based composites.[18]

As expected, the change in activation energy Δ_{ph} is not as pronounced as that of Δ_d due to a difference in mechanisms of dark and photoconductivity. The inset of Figure 7 shows the Arrhenius fits of the photoconductivity obtained in the composite **2**/C_{60} at an electric field of 20 V μm^{-1} and light intensity of 20 mW cm^{-2}. As seen from the comparison between dark and photoconductivity activation energies, the photoconductivity exhibits much weaker temperature dependence, which yields activation energies $\Delta_{ph} \approx 0.1 - 0.2$ eV below T_g and $\Delta_{ph} \approx 0.3 - 0.5$ eV above T_g.

As mentioned above, several mechanisms contribute to the photoconductivity temperature dependence, and more experiments are required to reveal the dominant mechanism. However, qualitative suggestions can be made on the basis of our results and studies on polymer composites reported in the literature. In PVK/C_{60} composites, the photogeneration efficiency was found to be independent of $T - T_g$.[18] DCDHF molecules are characterized by ionization potentials close in value to that of carbazole. Also, similarly to the PVK/C_{60} system, there is spectroscopic evidence of charge – transfer complex formation between DCDHF and C_{60} in the same wavelength region. Therefore, it is reasonable to assume that the mechanism of photogeneration in DCDHF/C_{60} glasses at a wavelength of 676 nm is similar to that of PVK/C_{60} composites at this wavelength. Since photogeneration efficiency does not depend on $T - T_g$,[18] it would not account for a change in activation energy Δ_{ph} at around T_g. Charge – carrier mobility (μ) exhibits a change in activation energy at T_g in polymers as a result of Brownian-motion onset in a liquid state.[64] However, at temperatures above T_g the activation energy obtained from mobility measurements *decreases* in contrast with Δ_{ph}. Therefore, among the factors contributing to a free charge density,[71] recombination and trapping are most likely responsible for the observed behavior to a greater extent than charge generation and transport.

2.5. Photorefractive Properties

2.5.1. Two-Beam Coupling

2.5.1.1. Steady State

The PR two-beam coupling gain coefficient (Γ) depends on the temperature through the effective electro-optic nonlinearity and imaginary part of the space – charge field (Im E_{sc}).[72] With p-polarized writing beams and relatively small internal inter-beam angles ($\cos\theta_{int} \approx 1$), the temperature dependence of the gain coefficient at temperatures above T_g can be represented as follows [Equation (10)]:

$$\Gamma(T) \sim [C_{BR}(T) + C_{EO}(T)]\mathrm{Im}E_{sc}(T) \quad (10)$$

where the coefficients C_{BR} and C_{EO} describe electric field-induced chromophore reorientation as introduced in Equation (5). In Section 2.5.2.1. we will consider separately possible temperature effects from chromophore reorientation [first multiplier in Equation (10)] and space – charge field (E_{sc}) in order to understand the overall temperature dependence of the gain coefficient.

The two-beam coupling gain coefficient (Γ) was measured as a function of electric field and temperature at a wavelength of 676 nm. Figure 8 shows the electric field dependence of the gain coefficient at various temperatures measured in the composite

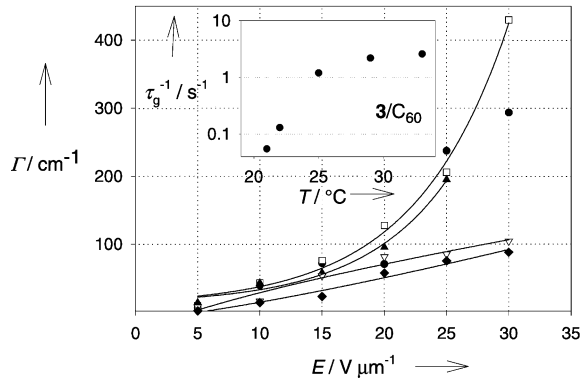

Figure 8. *Electric field dependence of the gain coefficient obtained in composite **3**/C_{60} at various temperatures (● 21 °C, □ 22 °C, ▲ 25 °C, ▽ 29 °C, ◆ 33 °C). Lines provide a guide for the eye. Inset shows the temperature dependence of the PR response time at an electric field of 30 V μm^{-1} and total writing beam intensity of 120 mW cm^{-2}.*

3/C_{60}. Already at several degrees above T_g the reduction of the gain coefficient is observed. As the temperature increases further ($\approx 6\,^{\circ}C$ above T_g), the gain coefficient decreases several times. Composites **1**/C_{60} and **2**/C_{60} exhibited similar trends – as the temperature increased above T_g, the gain coefficient substantially decreased over a small temperature region of $\approx 5-10\,^{\circ}C$ above T_g. Analysis of the contributions of the orientational transport and trapping processes to the observed behavior will be presented in Section 2.5.2.1.

2.5.1.2. Dynamics

The PR response speed (τ_g^{-1}) obtained from single-exponential fits to the gain factor [$\gamma \sim 1 - \exp(-\tau_g^{-1}t)$] in the composite **3**/C_{60} at an electric field of $30\,V\,\mu m^{-1}$ and total writing beam intensity of $120\,mW\,cm^{-2}$ as a function of temperature is shown in the inset of Figure 8. At temperatures close to T_g the PR response speed is similar to the orientational speed k_{BR} obtained in transmission ellipsometry experiments (Section 2.3.2.). As expected, the PR response speed increases dramatically with the temperature, reaching values of $\approx 2.6\,s^{-1}$ at $\approx 10\,^{\circ}C$ above T_g. However, the increase in PR response speed is not as large as that achieved in k_{BR} under similar conditions ($k_{BR} \approx 8\,s^{-1}$at $T_g + 10\,^{\circ}C$, Figure 5 b), due to the increasing role of photoconductivity in the PR response speed. The response speed τ_g^{-1} is a useful quantity in evaluation of the material for potential use in applications that utilize the beam coupling properties of the PR material. However, the gain signal is a complicated function of PR grating index modulation,[2] and therefore, the PR response speed does not directly reflect the properties of the PR grating. The four-wave mixing (FWM) technique allows direct probing of the PR grating, and thus, for more detailed evaluation of PR dynamical response we will concentrate on the PR grating dynamics obtained in a FWM experiment (Section 2.5.2.2.).

2.5.2. Four-Wave Mixing

2.5.2.1. Steady State

The diffraction efficiency (η) measured in FWM experiment is related to refractive index modulation Δn_{PR} of the PR grating as follows [Equation (11)]:[1]

$$\eta(T) \sim \sin^2[C\Delta n_{PR}(T)] \tag{11}$$

where C is a temperature-independent geometrical factor (see Experimental Section for details). The refractive index modulation can be represented as [Equation (12)]

$$\Delta n_{PR}(T) \sim f(T)\,|E_{sc}(T)| \tag{12}$$

where *f(T)* is an orientational factor, which is a function of the internal angles of incidence and the coefficients $C_{BR}(T)$ and $C_{EO}(T)$ defined in Equations (5).[1]

It is conventional[72–74] to apply Kukhtarev's model[75] in order to describe space – charge field formation in organic PR materials. In this model the absolute value of the space – charge field ($|E_{sc}(T)|$) is given by Equation (13)

$$|E_{sc}(T)| \sim \frac{\sigma_{ph}(T)}{\sigma_{ph}(T) + \sigma_d(T)} \frac{E_0 E_q(T)}{\sqrt{E_0^2 + E_q^2(T)}} \tag{13}$$

where E_0 is the projection of applied electric field along the grating wavevector and the saturation field $E_q(T) = e\Lambda N_T(T)/[2\pi\varepsilon_0\varepsilon(T)]$, where e is the charge, Λ is the grating constant, N_T is the PR trap density, and ε is the dielectric constant. Equation (13) assumes that the carrier drift in the electric field dominates the diffusion of carriers.

We now consider possible contributions of various temperature-dependent parameters in the refractive index modulation (Δn_{PR}) given by combining Equations (12) and (13). In keeping with our measurements of temperature dependence of dark and photoconductivity (Section 2.4.), the conductivity contrast $\sigma_{ph}/(\sigma_d + \sigma_{ph})$ decreases as the temperature increases due to a much stronger increase in dark conductivity compared with photoconductivity (Figure 6 and 7). The orientational factor $f(T)$ at temperatures above T_g is also a decreasing function of temperature (Section 2.3.1.). It is possible that, similar to polymer composites, the saturation field (E_q) also decreases as the temperature increases due to reduced trap density (N_T) at elevated temperatures.[74] We note that in the studied temperature range, the dielectric constant of DCDHF glasses does not depend on temperature and, therefore, does not contribute to the temperature dependence of the saturation field. The contribution of the saturation field $E_q(T)$ in the temperature dependence of Δn_{PR} depends on its magnitude relative to E_0. In keeping with our measurements of PR phase shift in DCDHF glasses, E_q is always lower than E_0 under our experimental conditions. Therefore, apart from the temperature dependence of the conductivity contrast, the primary temperature dependence of the space – charge field $|E_{sc}(T)|$ would originate in that of the saturation field $E_q(T)$ in the numerator of Equation (13). Similar considerations are applicable to the two-beam coupling gain coefficient given by Equation (10): the orientational factor and conductivity contrast decrease with temperature, and the temperature dependence of the imaginary part of the space – charge field ($\mathrm{Im}E_{sc}$) is similar to that of the saturation field (E_q) under our experimental conditions.

To further analyze the temperature dependence of steady-state two-beam coupling gain and diffraction efficiency, we consider the contributing factors separately. As discussed in Section 2.3.1., at temperatures up to $\approx T_g + (10-15)\,^{\circ}C$ the temperature dependence of the electric field-induced birefringence ($\Delta n_{BR}(T)$) does not significantly depart from that expected from the oriented gas (Figure 4), and therefore, can be considered as a contribution of orientational processes in the overall temperature dependence of steady-state PR modulation of refractive index. Figure 9 shows temperature dependence of the following parameters normalized at $T = T_g + 2\,^{\circ}C$: 1) steady-state birefringence Δn_{BR}; 2) conductivity contrast $\sigma_{ph}/(\sigma_d + \sigma_{ph})$ multiplied by Δn_{BR} (see Equations (12), (13)); 3) gain coefficient Γ; and 4) refractive index modulation calculated from diffraction efficiency – all measured in the composite **1**/C_{60} at temperatures $T_g < T < T_g + 17\,^{\circ}C$ and electric fields of 20 – $25\,V\,\mu m^{-1}$. If Kukhtarev's theory[75] is applicable, then the

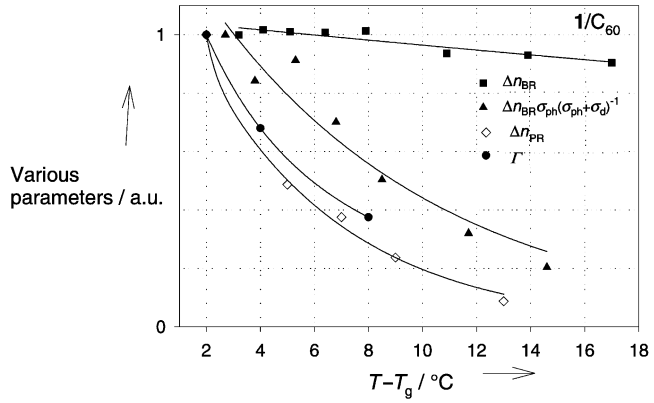

Figure 9. *Comparison of temperature dependencies of electric field-induced birefringence, conductivity contrast, two-beam coupling gain coefficient and PR grating index modulation in the compound* ***1****/C_{60}. Lines provide a guide for the eye.*

temperature dependence of the photoconductivity contrast and steady-state birefringence would account for most of the temperature dependence of the gain coefficient and Δn_{PR} (Figure 9). However, it is not clear whether Kukhtarev's theory can be applied in this study. Apart from mobility and charge-generation-efficiency dependence on the electric field, which are relatively easy to include in Equation (13),[18] a larger inconsistency could come from the inapplicable use of the conductivity contrast. In the derivation of Equation (13) for inorganic crystals, the donor sites are responsible for both dark conductivity (generation of free carriers by thermal ionization) and photoconductivity (light-induced ionization).[75] In organic PR materials with hole transport dominating, the function of the donors in inorganic crystals—generation of free carriers—is performed by acceptors, usually sensitizers (in our case C_{60}) introduced into the system. Thus, the photoconductivity in PR organics is due to light-induced ionization of the acceptor (sensitizer). However, in most cases, the dark conductivity is not related to the sensitizer, and therefore, cannot be introduced into Equation (13) through the conductivity contrast.

As mentioned above, it was previously shown[74] that the saturation field E_q was a decreasing function of temperature due to the reduction of PR trap density N_T with temperature in polymer composites, and similar trends are expected to be valid for DCDHF glasses. This effect would lead to a decrease in the space-charge field [Equation (13)]. However, the contribution of reduced trap density to the observed temperature dependence of the gain coefficient and refractive index modulation (Figure 9) cannot be evaluated quantitatively due to the questionable applicability of the Kukhtarev's model to organic materials with high dark conductivity. In addition to the conductivity contrast inconsistency discussed above, Equation (13) does not take into account either the contribution of injected charges[74] or ionic conduction, which are relevant in PR organic materials. Unfortunately, most existing PR models that do take into account photoelectric properties of polymers and therefore, better describe the PR effect in amorphous, organic materials,[19, 76] do not account for dark conductivity.

2.5.2.2. Dynamics

By analyzing the diffraction efficiency transients obtained from the FWM experiment, we assessed the PR grating formation and dark decay dynamics. The refractive index modulation Δn_{PR} was calculated from the measured diffraction efficiency using Equation (13), and the transient of $\Delta n_{PR}(t)$ was fitted with either single or stretched exponentials ($\Delta n_{PR} \sim 1-\exp(-\kappa_r t)$, $\Delta n_{PR} \approx 1-\exp[-(\kappa_r t)^{\beta}]$ or $\Delta n_{PR} \sim \exp(-\kappa_d t)$, $\Delta n_{PR} \sim \exp[-(\kappa_d t)^{\beta}]$), yielding a PR rise speed κ_r and a dark decay speed κ_d. Similar to the orientational dynamics observed in electric field-induced birefringence experiments (Section 2.3.2.) the refractive index modulation [$\Delta n_{PR}(t)$] time evolution is described well with a single-exponential function at temperatures above T_g. Figure 10a illustrates the data and the single-exponential fit obtained for the composite **3**/C_{60} at an electric field of 20 V μm^{-1}, a light intensity of 800 mW cm^{-2} and a temperature of 23 °C. To understand the factors limiting the PR speed in DCDHF glasses, we analyzed the intensity dependence of the PR rise dynamics.[20] Figure 10b shows PR rise speed κ_r obtained for the composite **3**/C_{60} as a function of the total writing beam intensity at various temperatures. At every temperature we fit the intensity dependences with a power law function ($\kappa_r \approx I^b$). At temperatures below T_g the intensity dependence of the PR speed is weak ($b \approx 0.23$), which is the sign of orientationally limited PR dynamics.[31, 32] The similarity between the PR rise

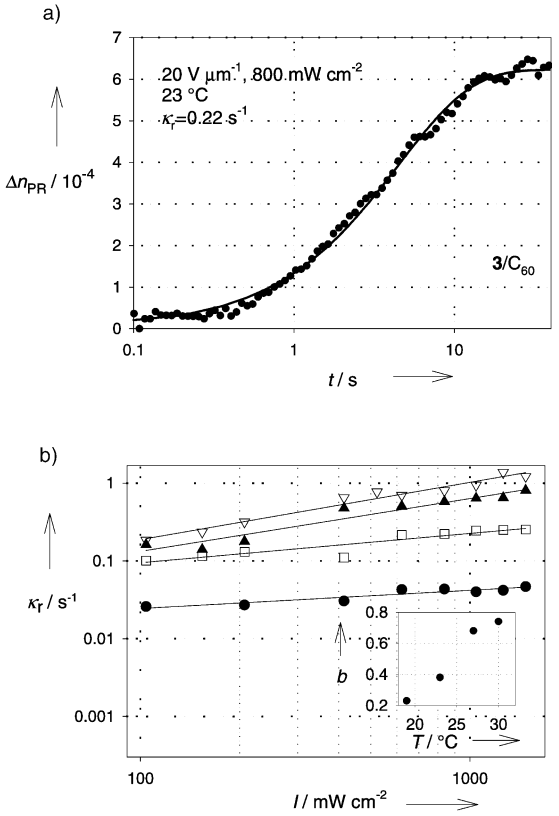

Figure 10. *a) PR grating time evolution observed in the composite* ***3****/C_{60} at 23 °C. Solid line (——) shows a single-exponential fit to the data. b) Intensity dependence of PR rise speed ($\kappa_r \approx I^b$) at various temperatures (● 19.5 °C, □ 23 °C, ▲ 27 °C, ▽ 30 °C) obtained in composite* ***3****/C_{60}. Inset shows temperature dependence of power law exponent (b).*

speed $\kappa_r \approx 0.025 - 0.045\ s^{-1}$ and the orientational speed $k_{BR} \approx 0.02\ s^{-1}$ at temperatures several degrees below T_g confirms this conclusion. As the temperature increases, the intensity dependence of the PR speed becomes stronger, with the power law exponent b increasing (inset of Figure 10b), which suggests that both orientational effects and photoconductivity contribute to the PR speed at temperatures above T_g.

The dark decay speed κ_d can provide information about the nature of shallow traps in the material, since in Schildkraut and Buettner's model[76] it is directly connected to the thermal detrapping rate.[71] However, in this model the dark conductivity, which becomes large at temperatures above T_g and may affect PR grating dark decay, is not taken into account. In DCDHF glasses, the dark decay speed (κ_d) is a strong function of the temperature relative to T_g (Figure 11), similar for all materials studied. Therefore, the observed dark decay is not related to the chemical nature of the glasses. However, further studies are necessary to separate the weak contribution of the temperature-dependent thermal detrapping from the strong contribution of $T - T_g$-dependent dark conductivity in the observed grating dark decay.

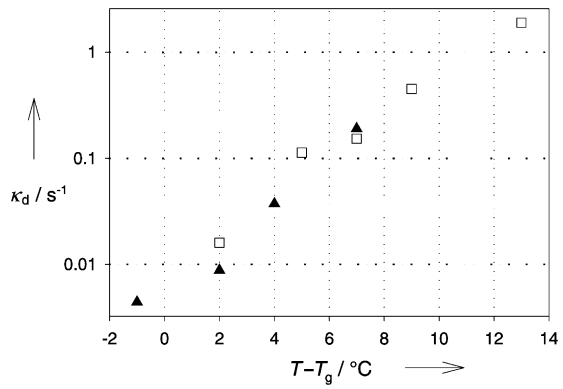

Figure 11. *Dependence of grating dark decay speed on relative to* T_g *temperature (□* ***1****/*C_{60}*, ▲* ***2****/*C_{60}*).*

3. Conclusions

We presented a comprehensive study of several low-molecular weight monolithic glasses containing DCDHF derivatives. Dielectric, birefringent, conductive, and PR properties were studied as a function of temperature.

Dielectric measurements of DCDHF glasses (Section 2.2.) reflected the highly polar nature of these materials and revealed a thermal behavior similar to that of polymers. At temperatures below T_g the secondary relaxation was detected in the higher frequency region ($\approx$10 kHz – 1 MHz) of the dielectric loss spectrum. At temperatures above T_g the secondary relaxation shifted to frequencies above 1 MHz, while a strong primary relaxation was observed at lower frequencies (10 mHz – 1 kHz, depending on the temperature) and attributed to a chromophore reorientation in the ac electric field. Havriliak – Negami fits of the dielectric permittivity revealed temperature-independent cooperativity in orientation at temperatures above T_g. Temperature dependence of dielectric relaxation times (τ_0) was described reasonably well by the WLF equation, with constants $C_1 = 12$ and $C_2 = 42$ K.

The steady-state values of electric field-induced birefringence (Section 2.3.1.) decreased as the temperature increased above T_g. The decrease was stronger than predicted by the oriented gas model, which was attributed to space – charge field effects due to increased dark conductivity.

The dynamics of the electric field-induced birefringence (Section 2.3.2.) was found to depend strongly on $T - T_g$. At temperatures below T_g, dispersive, birefringent transients were characterized by stretched exponentials with orientational speed $k_{BR} \approx 0.01 - 0.1\ s^{-1}$. At temperatures above T_g the transients were single-exponential, with orientational speed reaching values of $\approx 10\ s^{-1}$ at 10 °C above T_g.

The dark conductivity (Section 2.4.1.) was on the order of or below 0.1 pS cm^{-1} at an electric field of 20 V μm^{-1} at temperatures around T_g. However, it exhibited strong $T - T_g$ dependence, reaching values of $\approx$10 pS cm^{-1} at temperatures $\approx$20 °C above T_g. A large change in activation energy of dark conductivity from $\Delta_d \approx 0.7$ eV around T_g to $\Delta_d \approx 2 - 2.6$ eV above T_g was attributed to a thermal activation of ionic conduction at elevated temperatures.

The photoconductivity (Section 2.4.2.) was $\approx 0.4 - 2$ pS cm^{-1} at an electric field of 20 V μm^{-1} and light intensity of 20 mW cm^{-2} and weakly dependent on temperature. Similar to dark conductivity, the photoconductivity exhibited a change in activation energy near T_g, but the change was much less pronounced than in the case of dark conductivity and was attributed to a change in trapping and recombination processes.

The PR two-beam coupling gain coefficient and diffraction efficiency (Sections 2.5.1.1. and 2.5.2.1., respectively) decreased as the temperature increased above T_g. The decrease was attributed to thermal disruption of chromophore alignment, significantly increased dark conductivity, and reduced trap densities at elevated temperatures. A model that would implement the dark conductivity into space – charge field formation in PR organic materials is needed to fully explain the observed temperature dependence.

The PR rise speed (Section 2.5.2.2.), which characterizes the PR grating writing process, was orientationally limited and was on the order of $\approx 0.02 - 0.05\ s^{-1}$ at temperatures several degrees below T_g. As the temperature increased, the PR speed increased with the largest increase of $\approx$4 times over $\approx$3 °C in the temperature region around T_g. At higher temperatures the PR speed became photoconductivity-limited, as manifested through the stronger intensity dependence of the PR speed. As a result, the values of the PR speed, which are achieved at temperatures $\approx$10 °C above T_g, were $\approx 1 - 2\ s^{-1}$ at best, which is below the orientational speed k_{BR} observed under similar conditions.

In summary, DCDHF glasses exhibited large temperature sensitivity at temperatures around T_g. A considerable increase in PR speed can be achieved by changing the operating temperature or T_g of the DCDHF glass. The PR grating dark decay was found to be highly $T - T_g$ dependent, which allows for efficient thermal fixing/erasing of the grating by varying the temperature within 5 – 10 °C. The gain coefficient and diffraction efficiency

dramatically decrease as the temperature increases above T_g, which implies that the steady-state and dynamic properties are optimized at different temperatures. Therefore, the requirements for particular applications have to be taken into account in fine-tuning the properties using temperature. Moreover, for a particular application, careful temperature control of the sample will be essential to obtain repeatable and reproducible performance. In DCDHF glasses the best temperature region, in which the steady-state properties are still good, and the dynamic properties are significantly improved, was found to be from T_g to $\approx T_g + (2-3)\,^\circ$C. However, a PR model which takes into account dark conductivity in organic materials is needed to quantitatively describe the observed temperature dependencies and clarify the physical mechanism.

Experimental Section

1. Synthesis: A representative synthesis of the chromophores used in our temperature-dependence studies is provided in ref. [32]

2. Sample preparation: The samples contained 99.5 wt.% DCDHF chromophore and 0.5 wt.% C_{60}. The DCDHF chromophores and C_{60} were dissolved in benzene (50 mg mL^{-1} in the case of DCDHF and 1 mg mL^{-1} in the case of C_{60}), stirred, filtered through a 0.2 μm filter, and cast on indium tin oxide coated (ITO) slides. The films were dried overnight in an oven at 120 °C. When the residual solvent evaporated, the ITO slides with films were heated to a temperature slightly higher than the melting point of the chromophore (125–135 °C), sandwiched with 70–100 μm spacers, and quenched by placing the sample on a metal plate at room temperature. Such a procedure led to a formation of stable glass that maintained good optical quality over the period of at least eight months so far.

3. Temperature control: In dielectric, ellipsometric, dc conductivity, and PR measurements the sample was mounted on a temperature-controlled stage. The actual temperature was read out by a thermocouple attached to the sample surface, as close as possible to a light beam (when applicable). The accuracy of the temperature control was 0.1 °C in transmission ellipsometry and dc conductivity experiments, and 0.5 °C in dielectric and PR experiments. In all experiments the sample was allowed to equilibrate for 5 min at each temperature prior to taking data. Experiments were conducted in both heating and cooling modes. The measured quantities were independent of the mode or heating/cooling rate.

4. Dielectric spectroscopy: Real (ε') and imaginary (ε'') parts of the dielectric constant were measured as functions of frequency and temperature using a Solartron impedance/gain-phase analyzer. An ac electric field (0.1 Vpp) was applied to the sample, and the dielectric constant was measured as a function of frequency ranging from 10 mHz to 1 MHz. The experiment was repeated at various temperatures.

5. Conductivity: Photoconductivity was measured at the wavelength $\lambda = 676$ nm (Kr^+ laser) using a conventional dc technique. First, an electric field was applied to the sample. The dark current was measured after at least 60 s, allowing transient effects to disappear. Then the light beam was opened with a magnetic shutter, and the current was recorded. The photocurrent was calculated as the difference between total current in the presence of light and the dark current. The dark and photoconductivity were calculated using the formula $\sigma = iL/(VS)$, where i is dark or photocurrent, respectively, L is the sample thickness, V is the applied voltage, and S is the electrode area.

6. Birefringence: Electric field-induced birefringence was measured using a conventional transient ellipsometry technique. Light of wavelength $\lambda = 976$ nm (laser diode) was polarized at 45° with respect to the plane of incidence. The sample was placed between crossed polarizers at the angle of 30° between the sample normal and the light beam. The residual sample birefringence was compensated by a Soleil–Babinet compensator, so that no transmitted light could be detected in the absence of electric field. The electric field was applied to the sample with a rise time below 100 μs, and the intensity of transmitted light was recorded as a function of time, with time resolution below 100 μs. The birefringence was calculated using the formula given in Equation (14)

$$\Delta n = \frac{\lambda \cos\varphi}{2\pi L \sin^2\varphi} \arcsin\sqrt{I/I_{max}} \tag{14}$$

where λ is wavelength, φ is the internal angle of incidence, L is the sample thickness, and I_{max} is the maximal transmitted intensity.

7. Two-wave mixing: Two-wave mixing experiments were conducted at a wavelength of 676 nm (Kr^+ laser). The p-polarized beams were incident at external angles of 18° and 45° to the sample normal and the beam ratio was 1:1. The total writing beam intensity was 120 mW cm^{-2}. The electric field was applied so that the negative high voltage would be on the sample electrode facing the incident beams in order to minimize beam fanning and its related unphysical gain coefficients.[77] The beams were opened with a magnetic shutter (switching time below 150 μs), and the intensity of both amplified and depleted beams was monitored. After the measurements, the grating was erased by a larger diameter non-Bragg matched erasing beam. The gain coefficient was calculated using the formula given in Equation (15)

$$\Gamma = \frac{\cos\theta_1}{L} \ln\frac{\gamma}{2-\gamma} \tag{15}$$

where θ_1 is the smaller internal angle of incidence, L is the sample thickness, and $\gamma = I_{\text{with pump}}/I_{\text{without pump}}$.

8. Four-wave mixing: The experiment was conducted at $\lambda = 676$ nm (Kr^+ laser). The grating was written by two s-polarized beams incident at external angles of 18° and 45° to the sample normal and with beam ratio 1:1. The probe beam was p-polarized, had intensity on the order of 1% of the total writing beam intensity and was counterpropagating with one of the writing beams. The electric field was applied to the sample, the writing beams were opened with a magnetic shutter, and the diffracted beam was monitored as a function of time. When the diffracted signal reached a steady state, the writing beams were turned off, and the dark decay was recorded. The external diffraction efficiency (η) was calculated as a ratio of the diffracted (I_d) and incident (I_0) probe beam intensities: $\eta = I_d/I_0$. The PR grating refractive index modulation (Δn_{PR}) was calculated from diffraction efficiency (η) using the relation [Equation (16)]:[1]

$$\Delta n_{PR} = \frac{\lambda \arcsin\sqrt{\eta}}{\pi L \cos(\theta_2 - \theta_1)} \tag{16}$$

where λ is the wavelength, $\theta_{1,2}$ are internal angles of incidence of the writing beams, and $L = d/\sqrt{\cos\theta_1 \cos\theta_2}$, where d is the sample thickness.

We thank Prof. R. Wortmann for electroabsorption measurements of DCDHF glasses. Financial support from AFOSR Grant No. F49620-00-1-0038 is gratefully acknowledged.

[1] W. E. Moerner, A. Grunnet-Jepsen, C. L. Thompson, *Annu. Rev. Mater. Sci.* **1997**, *27*, 585 – 623.
[2] L. Solymar, D. J. Webb, A. Grunnet-Jepsen, *The Physics and Applications of Photorefractive Materials*, Clarendon Press: Oxford, **1996**.
[3] F. *J.* Chen, *Appl. Phys.* **1967**, *38*, 3418.
[4] K. Sutter, P. *J.* Gunter, *J. Opt. Soc. Am. B* **1990**, *7*, 2274 – 2278.
[5] S. Ducharme, J. C. Scott, R. J. Twieg, W. E. Moerner, *Phys. Rev. Lett.* **1991**, *66*, 1846 – 1849.
[6] K. Meerholz, B. Kippelen, N. Peyghambarian in *Photonic Polymer Systems* (Eds: D. Wise, G. Wnek, D. Trantolo, T. Cooper, J. Gresser) Marcel Dekker, Inc.: New York, **1998**.
[7] S. J. Zilker, *ChemPhysChem* **2000**, *1*, 72 – 87.
[8] W. E. Moerner, S. M. Silence, *Chem. Rev.* **1994**, *94*, 127 – 155.
[9] F. Wurthner, R.Wortmann, K. Meerholz, *ChemPhysChem* **2002**, *3*, 17 – 31.
[10] W. E. Moerner, S. M. Silence, F. Hache, G. C. Bjorklund, *J. Opt. Soc. Am. B* **1994**, *11*, 320 – 330.
[11] A. Grunnet-Jepsen, D. Wright, B. Smith, M. S. Bratcher, M. S. DeClue, J. S. Siegel, W. E. Moerner, *Chem. Phys. Lett.* **1998**, *291*, 553 – 561.
[12] D. Van Steenwinckel, E. Hendrickx, A. Persoons, K. Van den Broeck, C. Samyn, *J. Chem. Phys.* **2000**, *112*, 11 030 – 11 037.
[13] K. S. West, D. P. West, M. D. Rahn, J. D. Shakos, F. A. Wade, K. Khand, T. A. King, *J. Appl. Phys.* **1998**, *84*, 5893 – 5899.
[14] G. G. Malliaras, V. V. Krasnikov, H. J. Bolink, G. Hadziioannou, *Appl. Phys. Lett.* **1995**, *66*, 1038 – 1040.
[15] E. Hendrickx, D. Van Steenwinckel, A. Persoons, C. Samyn, D. Beljonne, J. L. Bredas, *J. Chem. Phys.* **2000**, *113*, 5439 – 5447.
[16] J. A. Herlocker, C. Fuentes-Hernandez, K. B. Ferrio, E.Hendrickx, P. A. Blanche, N. Peyghambarian, B. Kippelen, Y. Zhang, J. F. Wang, S. R. Marder, *Appl. Phys. Lett.* **2000**, *77*, 2292 – 2294.
[17] D. Van Steenwinckel, E. Hendrickx, C. Samyn, C. Engels, A. Persoons, *J. Mater. Chem.* **2000**, *10*, 2692 – 2697.
[18] T. K. Daubler, R. Bittner, K. Meerholz, V. Cimrova, D. Neher, *Phys. Rev. B* **2000**, *61*, 13 515 – 13 527.
[19] O. Ostroverkhova, K. D. Singer, *J. Appl. Phys.* **2002**, *92*, 1727 – 1743.
[20] D. Wright, M. A. Diaz-Garcia, J. D. Casperson, M. DeClue, W. E. Moerner, R. Twieg, J. *Appl. Phys. Lett.* **1998**, *73*, 1490 – 1492.
[21] D. Wright, U. Gubler, Y. Roh, W. E. Moerner, M. He, R. Twieg, J. *Appl. Phys. Lett.* **2001**, *79*, 4274 – 4276.
[22] K. Meerholz, B. L. Volodin, Sandalphon, B. Kippelen, N. Peyghambarian, *Nature* **1994**, *371*, 497 – 500.
[23] E. Hendrickx, D. Van Steenwinckel, A. Persoons, A. Watanabe, *Macromolecules* **1999**, *32*, 2232 – 2238.
[24] D. Van Steenwinckel, E. Hendrickx, A. Persoons, *Chem. Mater.* **2001**, *13*, 1230 – 1237.
[25] S. Schloter, A. Schreiber, M. Grasruck, A. Leopold, Kol'M. chenko, J. Pan, C. Hohle, P. Strohriegl, S. J. Zilker, D. Haarer, *Appl. Phys. B* **1999**, *68*, 899 – 906.
[26] Q. Wang, L. M. Wang, J. J. Yu, L. P. Yu, *Adv. Mater.* **2000**, *12*, 974 – 978.
[27] W. You, L. M. Wang, Q. Wang, L. P. Yu, *Macromolecules* **2002**, *35*, 4636 – 4645.
[28] P. M. Lundquist, R. Wortmann, C. Geletneky, R. J. Twieg, M. Jurich, V. Y. Lee, C. R. Moylan, D. M. Burland, *Science* **1996**, *274*, 1182 – 1185.
[29] Y. D. Zhang, L. M. Wang, T. Wada, H. Sasabe, *Appl. Phys. Lett.* **1997**, *70*, 2949 – 2951.
[30] L. M. Wang, M. K. Ng, L. P. Yu, *Appl. Phys. Lett.* **2001**, *78*, 700 – 702.
[31] O. Ostroverkhova, U. Gubler, D. Wright, W. E. Moerner, M. He, R. Twieg, *Adv. Funct. Mater.* **2002**, *12*, 621 – 629.
[32] U. Gubler, M. He, D. Wright, Y. Roh, R. Twieg, W. E. Moerner, *Adv. Mater.* **2002**, *14*, 313 – 317.
[33] O. Ostroverkhova, W. E. Moerner, M. He, R. J. Twieg, *Appl. Phys. Lett.* **2003**, *82*, 3602 – 3604.
[34] R. D. Dureiko, D. E. Schuele, K. D. Singer, *J. Opt. Soc. Am. B* **1998**, *15*, 338 – 350.
[35] A. Dhinojwala, G. K. Wong, J. Torkelson, *J. Chem. Phys.* **1994**, *100*, 6046 – 6054.
[36] D. B. Hall, A. Dhinojwala, J. Torkelson, *Phys. Rev. Lett.* **1997**, *79*, 103 – 106.
[37] P. Pretre, U. U. S. Meier, C. Bosshard, P. Gunter, P. Kaatz, C. Weder, P. Neuenschwander, U. W. Suter, *Macromolecules* **1998**, *31*, 1947 – 1957.
[38] A. R. Blythe, *Electrical properties of polymers*, Cambridge University Press: Cambridge (Engl.), New York, **1979**.
[39] S. Havriliak, S. Negami, *J. Polym. Sci.* **1966**, *14*, 99.
[40] E. Rossler, H. Sillescu, *Glasses and Amorphous materials*, Vol. 9, VCH Publishers, Inc.: New York, **1991**.
[41] G. P. Johari, M. Goldstein, *J. Chem. Phys.* **1970**, *53*, 2372.
[42] E. Riande, E. Saiz, *Dipole moments and birefringence of polymers*, Prentice Hall: Englewood Cliffs, NJ, **1992**.
[43] R. Wortmann, personal communication.
[44] S. R. Elliott, *Physics of amorphous materials*, Wiley: New York, **1990**.
[45] M. Kuzyk in *Characterization Techniques and Tabulations for Organic Nonlinear Optical Materials* (M. Kuzyk, C. Dirk), Vol. 60, Marcel Dekker, Inc.: New York, **1998**.
[46] P. Debye, *Polar Molecules*, The Chemical Catalog Company, Inc.: New York, **1929**.
[47] J. W. Wu, *J. Opt. Soc. Am. B* **1991**, *8*, 142 – 152.
[48] Sandalphon, B. Kippelen, K. Meerholz, N. Peyghambarian, *Appl. Opt.* **1996**, *35*, 2346 – 2354.
[49] C. H. Wang, S. H. Gu, H. W. Guan, *J. Chem. Phys.* **1993**, *99*, 5597 – 5604.
[50] C. H. Wang, *J. Chem. Phys.* **1993**, *98*, 3457 – 3462.
[51] M. A. Firestone, M. A. Ratner, T. J. Marks, W. P. Lin, G. K. Wong, *Macromolecules* **1995**, *28*, 2260 – 2269.
[52] S. Schussler, R. Richert, H. Bassler, *Macromolecules* **1994**, *27*, 4318 – 4326.
[53] M. He, R. Twieg, O. Ostroverkhova, U. Gubler, D. Wright, W. E. Moerner, *SPIE Proceedings* **2002**, *4802*, 9 – 20.
[54] M. Pope, C. E. Swenberg, *Electronic processes in organic crystals and polymers*, Vol. 56, Oxford University Press: New York, **1999**.
[55] S. Di Bella, G. Lanza, I. Fragala, S. Yitzchaik, M. A. Ratner, T. J. Marks, *J. Am. Chem. Soc.* **1997**, *119*, 3003 – 3006.
[56] M. Stahelin, D. M. Burland, M. Ebert, R. D. Miller, B. A. Smith, R. J. Twieg, W. Volksen, C. A. Walsh, *Appl. Phys. Lett.* **1992**, *61*, 1626 – 1628.
[57] J. Hooker, W. Burghardt, J. Torkelson, *J. Chem. Phys.* **1999**, *111*, 2779 – 2788.
[58] D. Jungbauer, I. Teraoka, D. Y. Yoon, B. Reck, J. D. Swalen, R. Twieg, C. G. Willson, *J. Appl. Phys.* **1991**, *69*, 8011 – 8017.
[59] I. Teraoka, D. Jungbauer, B. Reck, D. Y. Yoon, R. Twieg, C. G. Willson, *J. Appl. Phys.* **1991**, *69*, 2568 – 2576.
[60] S. Schussler, R. Richert, H. Bassler, *Macromolecules* **1995**, *28*, 2429 – 2438.
[61] S. Schussler, U. Albrecht, R. Richert, H. Bassler, *Macromolecules* **1996**, *29*, 1266 – 1268.
[62] M. Eich, H. Looser, D. Y. Yoon, R. J. Twieg, G. C. Bjorklund, J. C. Baumert, *J. Am. Opt. Soc.* **1989**, *6*, 1590 – 1597.
[63] A. Leopold, R. Bausinger, D. Haarer, J. Ostrauskaite, M. Thelakkat, *SPIE Proceedings* **2002**, *4802*, 33 – 41.
[64] P. M. Borsenberger, D. S. Weiss, *Organic photoreceptors for xerography*, Vol. 59, Marcel Dekker: New York, **1998**.
[65] R. Blum, M. Sprave, J. Sablotny, M. Eich, *J. Opt. Soc. Am. B* **1998**, *15*, 318 – 328.
[66] T. Miyamoto, K. Shibayama, *J. Appl. Phys.* **1973**, *44*, 5373.
[67] G. M. Sessler, B. Hahn, D. Y. Yoon, *J. Appl. Phys.* **1986**, *60*, 318 – 326.
[68] J. Vanderschueren, A. Linkens, *J. Appl. Phys.* **1978**, *49*, 4195 – 4208.
[69] E. Neagu, P. Pissis, L. Apekis, *J. Phys. D* **1997**, *30*, 1551 – 1560.
[70] A. Lian, L. Martinu, M. R. Wertheimer, *IEEE Trans. Dielectr. Electr. Insul.* **1995**, *2*, 62 – 73.
[71] Y. P. Cui, B. Swedek, N. Cheng, J. Zieba, P. N. Prasad, *J. Appl. Phys.* **1999**, *85*, 38 – 43.
[72] A. Grunnet-Jepsen, C. L. Thompson, W. E. Moerner, *J. Opt. Soc. Am. B* **1998**, *15*, 905 – 913.
[73] J. Zhang, K. D. Singer, *Appl. Phys. Lett.* **1998**, *72*, 2948 – 2950.
[74] R. Bittner, T. K. Daubler, D. Neher, K. Meerholz, *Adv. Mater.* **1999**, *11*, 123 – 127.
[75] N. V. Kukhtarev, V. B. Markov, S. G. Odulov, M. S. Soskin, V. L. Vinetskii, *Ferroelectrics* **1979**, *22*, 949 – 960.
[76] J. S. Schildkraut, A. V. Buettner, *J. Appl. Phys.* **1992**, *72*, 1888 – 1893.
[77] A. Grunnet-Jepsen, C. L. Thompson, R. J. Twieg, W. E. Moerner, *J. Opt. Soc. Am. B* **1998**, *15*, 901 – 904.

Received: December 31, 2002 [F633]

